Scilight

Health Informatics and Advanced Technologies
https://www.sciltp.com/journals/hiat



Cases Reports

Exploratory Thermal Heterogeneity Patterns in Pediatric Second-Degree Burns Using High-Resolution Infrared Thermography in Uruguay

Sergio Machado *,†, Beatriz Manaro †, Natalia Gryngras †, Georgina de Angelis †, Lizandra Gonzalez and Virginia Suarez

Burn and Reconstructive Surgery Unit, BRSU Pereira Rossell Hospital, UDELAR, Montevideo 11600, Uruguay
* Correspondence: smachado@hc.edu.uy
† These authors contributed equally to this work.

How To Cite: Machado, S.; Manaro, B.; Gryngras, N.; et al. Exploratory Thermal Heterogeneity Patterns in Pediatric Second-Degree Burns Using High-Resolution Infrared Thermography in Uruguay. *Health Informatics and Advanced Technologies* **2026**, *1*(1), 3.

Received: 18 April 2026
Revised: 20 August 2026
Accepted: 23 September 2026
Published: 6 November 2026

Abstract: Introduction: Early assessment of burn depth in pediatric patients remains a clinical challenge due to the heterogeneity of burn injuries and the dynamic changes that may occur during their evolution. Clinical assessment by an experienced surgeon remains fundamental; however, infrared thermography (IRT) may provide objective and complementary radiometric information through a rapid, non-invasive, non-contact, and non-ionizing technique. Objective: To describe the thermal distribution across the entire surface of second-degree burns in two pediatric patients using high-resolution infrared thermography and to explore the use of the 10th and 90th temperature percentiles (P10 and P90) and a normalized index derived from these percentiles, termed Thermal Heterogeneity by Percentiles (THP), as a descriptor of intralesional thermal heterogeneity. Methods: Two pediatric patients with second-degree burns were evaluated using a 320 × 240-pixel radiometric infrared sensor following a standardized bedside acquisition protocol. The entire clinically visible burn surface was delineated as the Whole Burn Region of Interest (WB-ROI). All radiometric temperature values contained within each WB-ROI were included in the analysis. Minimum temperature (Tmin), maximum temperature (Tmax), mean temperature (Tmean), median temperature, standard deviation (SD), interquartile range (IQR), coefficient of variation (CV), and the P10 and P90 percentiles were calculated. For exploratory purposes, THP = (P90 − P10)/P90 was calculated as a normalized measure of the separation between the lower and upper components of the intralesional thermal distribution. Results: The two cases showed different thermal distributions. Case 1 had a Tmean of 36.06 °C, SD of 0.59 °C, IQR of 0.93 °C, and CV of 1.63%, whereas Case 2 had a lower Tmean (34.38 °C) and greater thermal dispersion, with an SD of 0.97 °C, IQR of 1.27 °C, and CV of 2.83%. In Case 1, P10 and P90 were 35.34 °C and 36.88 °C, respectively, resulting in a THP of 0.042. In Case 2, P10 and P90 were 32.96 °C and 35.64 °C, respectively, resulting in a THP of 0.075. Case 2, which showed greater thermal dispersion and a higher THP, was independently classified at the bedside by the plastic surgery team as a deep partial-thickness burn, whereas Case 1 was clinically classified as a superficial-to-intermediate partial-thickness burn. Conclusions: Radiometric analysis of the WB-ROI, together with P10 and P90, enabled quantitative characterization of intralesional thermal heterogeneity while avoiding manual selection of hot and cold regions for index calculation. THP differed between the two cases and showed descriptive consistency with other measures of

Copyright: © 2026 by the authors. This is an open access article under the terms and conditions of the Creative Commons Attribution (CC BY) license (https://creativecommons.org/licenses/by/4.0/).
Publisher's Note: Scilight stays neutral with regard to jurisdictional claims in published maps and institutional affiliations.

thermal dispersion. However, these findings are exploratory and hypothesis-generating. THP should not currently be considered a validated marker of burn depth, healing potential, or prognosis, nor should it be used to establish diagnostic or therapeutic cutoff values. Its reproducibility and potential clinical significance should be prospectively evaluated in larger cohorts using independent clinical outcomes and established reference methods.

Keywords: infrared thermography; pediatric burns; thermal heterogeneity; deep partial-thickness burns

1. Introduction

The skin is the largest organ in the human body in terms of surface area and represents a fundamental barrier protecting internal tissues from mechanical injury, microbial infection, ultraviolet radiation, and extreme temperatures [1].

Burn injuries represent an important global health problem, particularly in children and in low- and middle-income countries. The epidemiology, mechanisms, severity, and outcomes of burn injuries vary considerably across geographical regions and socioeconomic settings [2]. A burn can be defined as a traumatic injury to the skin or other tissues resulting from thermal, chemical, electrical, or other forms of energy. Multiple classifications have been described according to burn depth and total body surface area involved, with burn depth having important implications for healing potential and treatment decisions [2,3].

Burns are commonly classified according to the anatomical depth of tissue involvement. First-degree burns involve the epidermis and generally heal spontaneously without permanent sequelae. Second-degree, or partial-thickness, burns involve the epidermis and variable portions of the dermis and may be classified according to the depth of dermal involvement. Superficial partial-thickness burns primarily involve the papillary dermis and generally show rapid spontaneous re-epithelialization. Intermediate partial-thickness injuries extend further into the dermis, whereas deep partial-thickness burns involve the deeper reticular dermis and may require longer healing times or surgical treatment. Full-thickness burns involve the entire thickness of the epidermis and dermis, resulting in the destruction of skin appendages and generally requiring surgical excision and skin grafting [4].

Among these categories, intermediate and deep partial-thickness burns may present particular diagnostic difficulties because their appearance and healing potential can evolve during the first days after injury. [5,6]. Clinical assessment by an experienced burn or plastic surgeon therefore remains fundamental, although objective imaging techniques have increasingly been investigated as complementary tools for burn-depth and healing-potential assessment [7,8].

Skin repair requires the coordinated interaction of multiple cell types and biological processes. The epidermis forms the outer protective barrier, while the dermis contains extracellular matrix, vascular structures, sensory receptors, glands, and skin appendages that contribute to tissue homeostasis and regeneration. Following injury, hemostasis, inflammation, angiogenesis, cellular proliferation, re-epithelialization, and tissue remodeling occur sequentially but with substantial temporal overlap. Surface temperature during this process may consequently be influenced by local blood flow, inflammation, tissue metabolism, heat transfer, and wound-healing dynamics [2,3].

Infrared thermography (IRT) has been investigated as a complementary imaging tool for burn assessment because it is non-invasive, non-contact, does not involve ionizing radiation, and enables rapid acquisition of surface-temperature information [3,7]. Thermographic assessment provides quantitative radiometric information regarding spatial temperature distribution, which may indirectly reflect physiological phenomena associated with local blood flow, inflammation, metabolism, and heat exchange [2–4].

Conventional visual assessment of burn wounds primarily evaluates morphological characteristics and does not directly quantify the physiological processes underlying tissue viability and healing potential. [5–7,9]. Several studies have therefore investigated thermal imaging as an adjunct to clinical examination for assessing burn depth and healing potential [7,8,10]. Thermographic findings should therefore be interpreted within the physiological and clinical context of the burn wound. [11–18].

The clinical application of infrared imaging has expanded substantially, including applications in wound assessment, vascular disorders, reconstructive surgery, and burn care [17–19]. Appropriate interpretation requires consideration of the physiological and technical determinants of skin temperature. Skin surface temperature may vary according to blood flow, anatomical location, autonomic activity, environmental conditions, acquisition

technique, and individual physiological characteristics [3,6,9]. Standardization of image acquisition and radiometric analysis is therefore particularly important when quantitative comparisons are performed [6,9].

Clinical examination remains the most widely available method for initial burn-depth assessment. However, visually determining the extent of tissue injury may be challenging, particularly in heterogeneous partial-thickness burns and during the early phase, when burn depth may evolve. Objective imaging techniques have consequently been investigated to complement, rather than replace, clinical judgment [4,5,7]. Among these techniques, Laser Doppler Imaging (LDI) has been extensively studied and is FDA-approved for the objective assessment of burn wound perfusion and healing potential, whereas infrared thermography (IRT) has emerged as a potential alternative, providing a rapid, non-contact, and non-ionizing assessment of skin surface temperature distribution. It should be noted that, to date, LDI is not available for use in burn centers in Uruguay. [18]. Unlike LDI, IRT does not directly measure microvascular blood flow; instead, it characterizes radiometric surface temperature patterns that may indirectly reflect physiological processes related to local perfusion, inflammation, metabolism, and heat exchange. [19] Studies comparing IRT with LDI and clinical healing outcomes have demonstrated associations between thermographic findings, burn depth, and healing potential [17–20].

More recent systematic reviews and meta-analyses support the potential diagnostic value of IRT, while also highlighting the methodological heterogeneity of the available studies and the need to standardize image acquisition, radiometric analysis, and interpretation [20].

This issue is particularly relevant in pediatric patients, in whom rapid, non-contact imaging may offer practical advantages. Thermal imaging has previously been investigated for pediatric acute burn-depth assessment [14], and recent studies using portable infrared devices, including the FLIR ONE Pro, further support its potential as an adjunctive bedside technique [21–23].

In this context, the present study describes the bedside application of high-resolution infrared thermography in two pediatric patients with second-degree burns. Rather than relying exclusively on visually selected hot and cold subregions, the complete radiometric temperature distribution of the Whole Burn Region of Interest (WB-ROI) was analyzed. The 10th and 90th temperature percentiles (P10 and P90) were subsequently explored as objective descriptors of intralesional thermal heterogeneity and used to derive an exploratory (Thermal Heterogeneity Patterns) THP.

Objective

Describe the thermal patterns observed using high-resolution infrared thermography in two pediatric patients with second-degree burns and to present thermal heterogeneity patterns (THP) as an exploratory metric for potential perfusion changes in burn wounds, within a pediatric burn and reconstructive surgery referral unit in Uruguay.

2. Materials and Methods

This descriptive case series was conducted at the Burn and Reconstructive Surgery Unit, Pereira Rossell Pediatric Hospital, Montevideo, Uruguay. Upon admission, each patient was jointly evaluated by the plastic surgery team and a certified medical thermologist before initiation of routine wound care by the nursing staff. Infrared thermographic images were acquired within the first 48 h after burn injury using a standardized institutional Thermal Burn Protocol (TBP). To minimize environmental and handling-related variability, wound dressings were removed only during the scheduled dressing change, avoiding unnecessary manipulation before image acquisition. After dressing removal, patients remained at rest for 10 min to allow thermal stabilization before imaging. Patient positioning was standardized according to burn location (upper limb, lower limb, or thorax). Thermal images were acquired at a fixed distance of approximately 30 cm using frontal and complementary lateral views when required by the wound topography. Image acquisition followed the point-of-care recommendations of the American Academy of Thermology, the Glamorgan protocol, and the standardized thermal window methodology proposed by the Uruguayan Association of Medical Thermology. All examinations were performed using a FLIR E75® infrared camera (Teledyne FLIR, Wilsonville, OR, USA), with an infrared detector resolution of 320 × 240 pixels (76,800 temperature measurement points), thermal sensitivity (NETD) of <40 mK (0.04 °C), spectral range of 7.5–14 µm, frame rate of 30 Hz, and a 24° × 18° field of view using the 17-mm lens. Camera emissivity was set to 0.98, corresponding to human skin. A fixed Rainbow color palette and a predefined thermal scale (31–38 °C) were used throughout the study to facilitate visual comparison among serial examinations. The color palette served exclusively for qualitative visualization, whereas all quantitative analyses were performed using radiometric temperature data extracted from the thermal images. Written informed consent was obtained from the legal guardians of all patients before image acquisition. The study protocol was approved by the Ethics Committee of Pereira Rossell Pediatric Hospital and registered with the Ministry of Public Health of Uruguay.

The present report constitutes an exploratory descriptive analysis within an ongoing prospective research project conducted by the the Burn and Reconstructive Surgery Unit (BRSU) research group.

2.1. Thermal Image Acquisition

Thermal image acquisition and storage were performed using Vision Fy® Thermal software (version 1.2.1). Radiometric image analysis was conducted using FLIR Research Studio® software (version 3.0.1). All thermal images were obtained by a trained thermologist following a standardized acquisition protocol at a fixed distance of approximately 30 cm from the wound surface by Thermal Burn Protocol (TBP). The camera emissivity was set to 0.98, corresponding to human skin. The infrared camera had undergone manufacturer calibration and blackbody verification before the study period. Patients remained at rest after dressing removal for 10 min before image acquisition. A fixed thermal scale ranging from 31 °C to 38 °C was applied to all thermograms to facilitate qualitative comparison throughout follow-up. In Case 1 and Case 2, the thermal images were obtained within the first 72 hours post-burn. Although camera distance and acquisition protocol (TBP) were standardized, ambient airflow and angular tolerance were not specifically controlled and are recognized as methodological limitations.

2.2. Thermal Image Analysis

To reduce observer-dependent variability, thermal analysis was performed using a Whole Burn Region of Interest (WB-ROI) encompassing the entire clinically visible burn surface. The burn boundary was delineated using the corresponding clinical photograph, previously aligned with the thermal image, in conjunction with the bedside plastic surgeon. This approach allowed all radiometric temperature values contained within the clinically defined burn area to be included in the analysis, avoiding the subjective selection of isolated hot or cold regions. Radiometric temperature values were extracted directly from the thermal dataset generated by the infrared sensor. The high-contrast rainbow palette was used exclusively for qualitative visualization of the spatial thermal distribution and was not used to define temperature thresholds or select regions for quantitative analysis. Within each WB-ROI, descriptive thermal parameters were calculated, including maximum temperature (Tmax), minimum temperature (Tmin), mean temperature (Tmean), median temperature, standard deviation (SD), interquartile range (IQR), and coefficient of variation (CV). To objectively characterize the lower and upper components of the intralesional thermal distribution, the 10th (P10) and 90th (P90) temperature percentiles were calculated using all radiometric temperature values contained within each WB-ROI. P10 was defined as the temperature below which 10% of the WB-ROI temperature values were distributed, whereas P90 represented the temperature below which 90% of the values were distributed. Thus, the interval between P10 and P90 represented the central 80% of the intralesional thermal distribution. The P10 and P90 values were derived mathematically from the complete radiometric dataset of each WB-ROI and were not determined by visual inspection of the pseudocolor thermogram or by manual selection of low- or high-temperature subregions. For exploratory purposes, a normalized (Thermal Heterogeneity Patterns) THP was calculated from these percentiles according to the following equation: as $(P90 - P10)/P90$.

The THP was considered a dimensionless descriptor of the relative thermal spread between the lower and upper percentiles of the intralesional temperature distribution. Higher THP values represent a greater normalized separation between P10 and P90, whereas lower values represent a narrower thermal distribution. Given the descriptive two-case design of the present study, the THP was used exclusively as an exploratory measure of intralesional thermal heterogeneity. It was not considered a validated measure of tissue perfusion, burn depth, healing potential, or prognosis, and no diagnostic or therapeutic cutoff values were established.

2.3. *Exploratory Perfusion Analysis*

The (Thermal Heterogeneity Patterns) THP was investigated as an exploratory quantitative descriptor of intralesional thermal heterogeneity. The index was calculated exclusively from radiometric temperature measurements extracted from the thermal images. Because of the limited number of patients included, THP is presented solely as an exploratory parameter intended to describe thermal perfusion patterns and should not be interpreted as a validated diagnostic or prognostic index. Only descriptive statistical analyses were performed. Temperature distributions were summarized using mean, median, maximum, minimum, and dispersion measures. Graphical representations were generated using the Pandas, NumPy, and Matplotlib libraries.

Case 1: Medical History: 9-month-old infant, good growth and development. Reason for admission: Major burn, burn from hot water from an electric kettle (approximately one liter), while being moved in a walker. Upon arrival at the emergency room, cold compresses were applied, an IV was inserted, and intravenous morphine was administered.

The burn described was on the face, lips, mouth, right shoulder and arm, back, and anterior chest (Figure 1C). Fluid resuscitation was performed. Subsequently, admission to BRSU was coordinated due to the extent of the injuries and involvement of a special area. Clinical examination revealed a second-degree intermediate burn on the face, cheek, lips, gums, and right upper eyelid. A total body surface area (TBSA) of 15% was observed. Thermal imaging was performed at the bedside with the plastic surgery team. Stable hemodynamics, heart rate of 130 bpm, otherwise normal, pain controlled with morphine, received an intervention through dermabrasion and escharectomy of the right upper limb, good subsequent evolution.

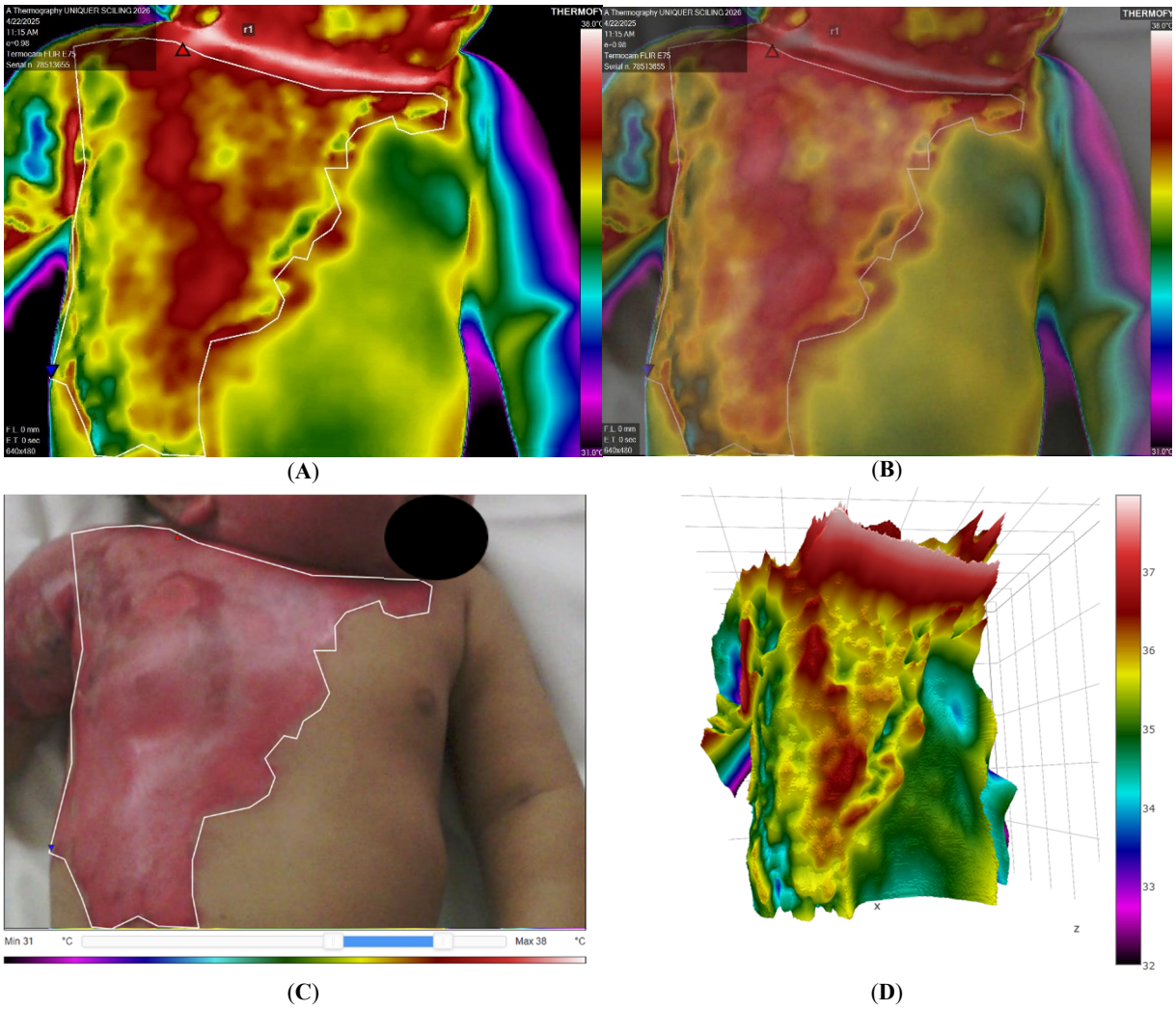


Figure 1. Case 1. Frontal thoracic thermal window (**A**–**C**). The Whole Burn Region of Interest (WB-ROI)**,** analyzed by the thermology team in conjunction with the plastic surgery team, is shown. The thermal distribution across the entire WB-ROI is represented, with lower- and higher-temperature regions qualitatively visualized using the rainbow high-contrast palette. (**D**) Three-dimensional representation of the radiometric surface-temperature distribution, illustrating spatial thermal heterogeneity across the entire burn wound.

Case 2: SM, 8 years old. Medical history: sialoidosis syndrome. Hypomyelination, non-paretic global hypotonia, strabismus, and risk of malignant hyperthermia. Admitted in December 2024, transferred from a tertiary care hospital due to a hot water burn on both thighs. On admission, deep partial-thickness burns were found on both thighs, with an estimated 7% of the body surface area (BSA) burned (Figure 2C). Hospitalization was decided upon for wound care. On the fourth day, a bedside thermography was performed with the plastic surgery team. Given the persistence of a thick eschar, follow-up surgery was scheduled, during which an escharotomy and autograft were performed. On the fourth day, the first dressing change was performed, revealing adherent and viable grafts, with an open wound remaining. The patient was temporarily discharged on 30 December and readmitted on 1 January 2025 for a second surgery on 2 January, during which an autograft was performed on the open wound, good subsequent evolution.

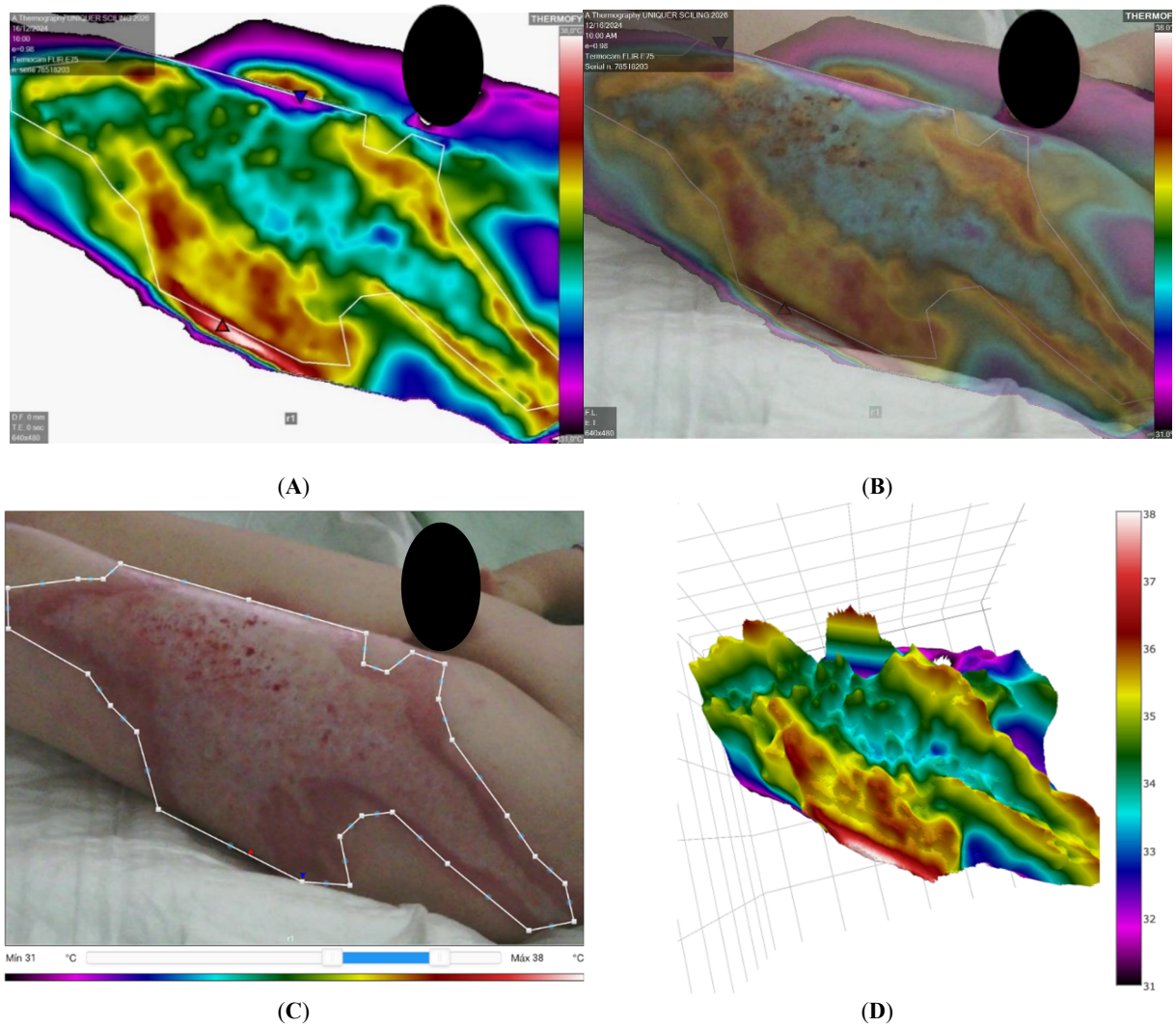


Figure 2. Case 2: Lateral thermal window (**A**–**C**): ROI profile analyzed by the thermology team, together with plastic surgeons. The thermal distribution across the Whole Burn Region of Interest (WB-ROI) is shown. Lower- and higher-temperature regions are qualitatively visualized using the high-contrast rainbow palette. (**D**): Three-dimensional representation of the radiometric surface-temperature distribution, illustrating spatial thermal heterogeneity across the burn wound.

3. Results

High-resolution infrared images were obtained at the bedside in both pediatric patients according to the Thermal Burn Protocol. Frontal and lateral thermal windows were acquired according to burn location and clinical accessibility. Thermal images showed spatial variations in surface temperature across the burn wounds, which were qualitatively visualized using the rainbow high-contrast palette. However, quantitative analysis was performed exclusively using radiometric temperature data, independently of the pseudocolor representation. For quantitative analysis, the entire clinically delineated burn surface was defined as the Whole Burn Region of Interest (WB-ROI). All radiometric temperature values contained within the WB-ROI were included in the descriptive analysis, rather than individually selecting small hot or cold regions based on their visual appearance (Figures 1 and 2).

3.1. Thermal Characteristics of the Whole Burn ROI (WB-ROI)

The two cases showed different thermal distributions within the WB-ROI. In Case 1, the mean temperature (Tmean) was 36.06 °C, with a median of 36.03 °C, a minimum temperature (Tmin) of 34.57 °C, and a maximum temperature (Tmax) of 37.55 °C. Thermal dispersion showed a standard deviation (SD) of 0.59 °C, an interquartile range (IQR) of 0.93 °C, and a coefficient of variation (CV) of 1.63%. In Case 2, the mean temperature was lower (34.38 °C), with a median of 34.43 °C, Tmin of 31.85 °C, and Tmax of 36.26 °C. Thermal dispersion was greater than that observed in Case 1, with an SD of 0.97 °C, an IQR of 1.27 °C, and a CV of 2.83%. Therefore, from a

descriptive perspective, Case 2 showed a broader and more heterogeneous intralesional thermal distribution than Case 1, with lower central temperature values and greater temperature dispersion within the WB-ROI (Table 1).

3.2. Percentile-Based Analysis of the WB-ROI

To objectively characterize the lower and upper components of the intralesional thermal distribution, the 10th (P10) and 90th (P90) percentiles were calculated using all radiometric temperature values contained within each WB-ROI. In Case 1, P10 was 35.34 °C and P90 was 36.88 °C, resulting in an absolute P90−P10 difference of 1.54 °C (Figure 3). In Case 2, P10 was 32.96 °C and P90 was 35.64 °C, resulting in a P90−P10 difference of 2.68 °C. Therefore, Case 2 showed a greater separation between the lower and upper ends of its intralesional thermal distribution (Figure 3). For graphical representation, the lower and upper thermal components were defined using the P10 and P90 thresholds, respectively. These percentile-based groups were mathematically derived from the complete temperature distribution of the WB-ROI and were not manually selected according to thermogram color or visual appearance.

3.3. Exploratory Thermal Heterogeneity Patterns

For exploratory purposes, the Thermal Heterogeneity Patterns (THP) was calculated from the P10 and P90 values using the following equation: $THP = (P90 - P10)/P90$.

Case 1 showed a THP of 0.042, whereas Case 2 showed a higher THP of 0.075 (Table 2). The higher THP observed in Case 2 was accompanied by greater descriptive thermal dispersion, as also reflected by its higher SD, IQR, and CV values. Bedside clinical assessment was performed independently by the plastic surgery team. Case 1 was clinically classified as a superficial-to-intermediate partial-thickness burn, whereas Case 2 was classified as a deep partial-thickness burn. Due to the descriptive design limited to two cases, no statistical analysis of the association between clinical burn-depth classification and THP was performed. Therefore, the THP values reported in this study should be considered exploratory descriptive findings and were not used to establish burn-depth categories, diagnostic thresholds, or therapeutic cutoffs.

Table 1. Descriptive thermal parameters obtained from the Whole Burn Region of Interest (WB-ROI) in Cases 1 and 2. All parameters were calculated from radiometric temperature values contained within the complete burn ROI. Tmin, minimum temperature; Tmean, mean temperature; Tmedian, median temperature; Tmax, maximum temperature; SD, standard deviation; IQR, interquartile range; CV, coefficient of variation.

Thermal Parameter	Case 1	Case 2
Tmin (°C)	34.57	31.85
Tmean (°C)	36.06	34.38
Tmedian (°C)	36.03	34.43
Tmax (°C)	37.55	36.26
SD (°C)	0.59	0.97
IQR (°C)	0.93	1.27
CV (%)	1.63	2.83

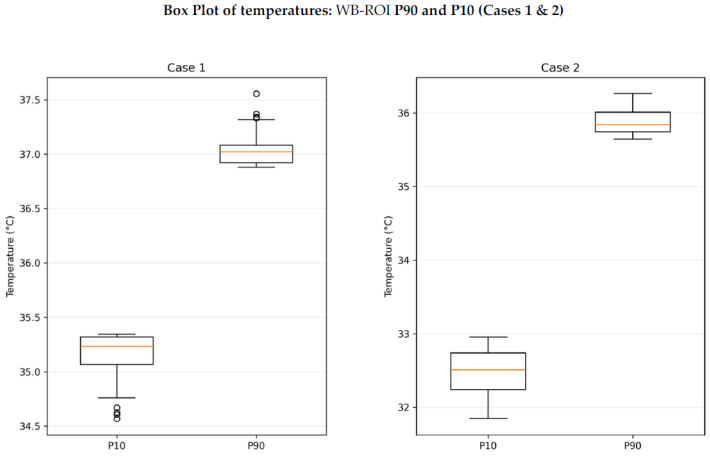


Figure 3. Distribution of P10 and P90 temperatures within the Whole Burn Region of Interest (WB-ROI) in Cases 1 and 2.

Box plots represent the distribution of radiometric temperature values corresponding to the lower (P10) and upper (P90) thermal percentiles of the (WB-ROI). The central line within each box represents the median, the box represents the interquartile range (IQR), and the whiskers indicate the range excluding outliers. Case 2 shows a greater separation between P10 and P90 than Case 1, reflecting greater intralesional thermal heterogeneity. These percentile distributions were derived from radiometric temperature data and were not based on visually selected hot or cold regions (Table 2). For exploratory purposes, THP was calculated from the radiometric temperature distribution of the entire burn ROI as the normalized difference between the 90th and 10th temperature percentiles: THP = (P90 − P10)/P90. The index was used solely as a descriptive measure of intralesional thermal heterogeneity and was not interpreted as a validated marker of tissue perfusion, burn depth, healing potential, or prognosis.

Table 2. Exploratory thermal parameters derived from the radiometric temperature distribution of the Whole Burn Region of Interest (WB-ROI). P10 and P90 represent the 10th and 90th percentiles of the complete intralesional temperature distribution, respectively. The exploratory Thermal Heterogeneity Patterns was calculated as (P90 − P10)/P90. THP is presented as a descriptive, hypothesis-generating parameter and not as a validated diagnostic index of burn depth.

(WB-ROI)	Case 1	Case 2
P10 (°C)	35.34	32.96
P90 (°C)	36.88	35.64
P90−P10 (°C)	1.54	2.68
THP	0.042	0.075

4. Discussion

Early assessment of burn depth and healing potential continues to represent a clinical challenge, particularly in the early stages, due to the dynamic nature of the injury and the possibility of wound conversion [3,4,8,10].

Clinical assessment performed by an experienced surgeon at the bedside continues to be fundamental at BRSU. In this context, different imaging methods, including Laser Doppler Imaging (LDI) and Infrared Thermography (IRT), have been studied as complementary tools to provide objective information about the injury [4,17,19]. In Uruguay, LDI is not available; therefore, the research team is conducting studies with high-resolution sensors and low-cost sensors such as the FLIR One Pro. [4,18,19].

The available evidence supports the potential of IRT to complement the clinical assessment of burns. In the meta-analysis by Asif et al., which included six studies and 197 burns or analyzed regions, thermography showed a pooled sensitivity of 84% and a specificity of 76% for differentiating superficial and deep burns [19]. A subsequent systematic review by Pedrosa et al., which included 15 studies, found an overall accuracy of 84.8%, with a sensitivity of 63% and a specificity of 81.9%, concluding that IRT has moderate accuracy and that its results should be interpreted with caution [20]. These findings support the interest in thermography as a complementary method, but they also highlight the need to improve the standardization of acquisition through thermal image acquisition protocols and interpretation by a medical thermologist for image analysis, as well as the use of validated software for human thermography.

From a pathophysiological perspective, the surface temperature of a burn depends on multiple factors, including the integrity of the dermal vascular plexus, local blood flow, the inflammatory response, tissue metabolism, and heat loss through evaporation. Areas with relatively preserved microcirculation may exhibit higher temperatures due to vasodilation and hyperemia, whereas progressive impairment of dermal perfusion may be associated with lower surface temperatures. Evaporation from the surface of an open wound constitutes another potential cooling mechanism. Therefore, the thermal differences observed in a burn likely reflect the interplay of multiple physiological processes, rather than solely the anatomical depth of the injury [4,17]. This is because such differences can produce artifacts that may influence the interpretation of the thermogram by inexperienced researchers or in the absence of strict protocols for bedside image acquisition.

In humans, several studies have demonstrated associations between the thermal characteristics of burns and their depth or healing potential. A systematic review that included 19 studies found significant correlations between IRT and LDI in the four clinical studies that compared both methods, while four of five studies evaluating healing time reported statistically significant associations with thermographic findings [3]. Similarly, validation studies have used time to healing, healing-potential categories, and LDI as references for interpreting temperature differences observed by thermography [4,14].

LDI is one of the most extensively studied objective methods for assessing the healing potential of burns. Unlike thermography—which measures infrared radiation emitted from the surface, providing an indirect representation of phenomena related to perfusion and heat exchange—LDI directly evaluates the movement of

erythrocytes via the Doppler effect. However, its technical requirements, cost, limited availability, and sensitivity to movement can restrict its use, particularly in children. Infrared thermography (IRT) offers practical advantages: it is a rapid, non-ionizing, and non-contact technique that can cover larger burn areas. It serves as a valuable complement when performed at the bedside by a physician specializing in medical thermology in collaboration with plastic surgeons. It is time-efficient and allows for repeated assessments—both in static mode (thermograms) and dynamic mode (video recordings)—which is particularly useful for very young or painful-experiencing children who may move during a physical examination. These characteristics are of particular interest when dealing with the pediatric population.

Recent pediatric evidence reinforces this possibility. A prospective pilot study published in 2026 evaluated the FLIR ONE Pro camera for pediatric burn-depth assessment and concluded that thermography has potential as a complementary portable tool, particularly in settings where LDI is not available [21]. Likewise, a recent systematic review of pediatric applications of IRT reported promising results for burn assessment, although it highlighted that the available studies remain small and methodologically heterogeneous [22]. Consequently, standardization of the acquisition protocol and radiometric analysis remains a fundamental element that may limit data reliability.

Most previous studies of thermography in burns have used absolute temperature differences (ΔT) between the lesion and an area of healthy skin as a reference [4,14,17,18]. This method is simple and intuitive and has made it possible to relate certain ΔT values to categories of healing potential. However, absolute skin temperature varies according to anatomical region and may be modified by environmental factors, acquisition distance, emissivity, sensor characteristics such as thermal sensitivity, and random selection of the region of interest. These variables should be considered particularly when comparing lesions located in different anatomical regions. [11,13].

In 2024, de Haan et al. evaluated the implementation of thermography in a specialized burn center using ΔT and healing-potential categories, demonstrating the feasibility of incorporating this technology into the clinical workflow, although they identified difficulties related to implementation and interpretation of the results [23]. In parallel, recent developments in image processing and predictive models show a trend toward quantitative and automated analysis of the entire lesion. Rangaiah et al. proposed in 2025 an approach based on advanced image processing, segmentation, and machine-learning models to reduce the subjectivity of conventional burn assessment [24]. These developments conceptually support the need to move from the selection of small representative regions toward methods that use a greater proportion of the information contained in the image.

In this regard, the present study used the Whole Burn Region of Interest (WB-ROI), corresponding to the entire clinically visible surface of the burn, as the unit of analysis. All radiometric values contained within this region were included in the quantitative analysis. This strategy allowed characterization of the complete intralesional thermal distribution and reduced dependence on small hot or cold regions selected subjectively.

The two cases showed different thermal patterns. Case 1 had a mean temperature of 36.06 °C, a median of 36.03 °C, Tmin of 34.57 °C, and Tmax of 37.55 °C. Thermal dispersion was relatively limited, with an SD of 0.59 °C, IQR of 0.93 °C, and CV of 1.63%. In contrast, Case 2 showed a lower mean temperature (34.38 °C), median of 34.43 °C, Tmin of 31.85 °C, and Tmax of 36.26 °C, accompanied by greater thermal dispersion, with an SD of 0.97 °C, IQR of 1.27 °C, and CV of 2.83%. Therefore, from an exclusively descriptive perspective, Case 2 showed a more heterogeneous intralesional thermal distribution than Case 1.

To quantify this heterogeneity without subjectively selecting hot and cold areas, the 10th and 90th percentiles of the complete temperature distribution of each WB-ROI were analyzed. P10 represents the lower thermal end of the intralesional distribution, and P90 represents the upper end. Both values are mathematically obtained from the radiometric data of the entire lesion; therefore, their determination does not depend on the visual selection of a region considered to have low or high perfusion.

Case 1 had a P10 of 35.34 °C and a P90 of 36.88 °C, resulting in a THP of 0.042. Case 2 had a P10 of 32.96 °C and a P90 of 35.64 °C, with a THP of 0.075. Therefore, Case 2 showed a greater normalized separation between the lower and upper ends of its thermal distribution. This result was consistent with its higher SD, IQR, and CV values, providing descriptive consistency to the interpretation of the THP as a possible measure of intralesional thermal heterogeneity. [23–26].

A clinically interesting finding was that Case 2, which showed the highest THP (0.075) and the greatest thermal dispersion, had been classified at the bedside by the plastic surgery team as a deep partial-thickness burn, whereas Case 1, with a lower THP (0.042) and lower thermal heterogeneity, was clinically considered a second-degree intermediate burn**.** This correspondence is of interest as a hypothesis-generating observation, but the design and number of patients in the present study do not allow an association between THP and burn depth to be established. [25–28].

For this reason, the THP should not currently be interpreted as a validated index of burn depth or as a direct measurement of perfusion. Consequently, the term "perfusion loss" will need to be validated through comparison with clinical outcomes and independent reference methods in a cohort that is currently being conducted by the research team. See Appendix A. Raw Thermal Image IRS and Profile Selection.

5. Conclusions

As of 2024, at the Burn and Reconstructive Surgery Unit of the Pereira Rossell Pediatric Hospital, the bedside clinical assessment of burn wounds in pediatric patients is supplemented by infrared thermography, performed by a medical thermologist in collaboration with experienced plastic surgeons.

In the two cases presented, high-resolution infrared thermography enabled quantitative characterization of the thermal distribution across the entire surface of the second-degree burns. Burn-depth assessment in pediatric patients is particularly challenging because of the heterogeneous nature of burn injuries, thinner skin, and dynamic physiological changes occurring during the acute phase, including early alterations in local perfusion. [4,17,19,24]

Radiometric analysis of the Whole Burn Region of Interest (WB-ROI), together with the P10 and P90 percentiles, enabled objective characterization of intralesional thermal heterogeneity. The exploratory THP derived from these percentiles showed different values in Cases 1 and 2 and was consistent with other descriptive measures of thermal dispersion. Clinically, Case 2, which showed greater thermal heterogeneity and a higher THP, was independently classified at the bedside by the plastic surgery team as a deep partial-thickness burn, whereas Case 1 was clinically classified as a second-degree intermediate burn. [4,24,27].

These findings are exploratory and hypothesis-generating. At present, the THP should not be considered a validated marker burn depth, healing potential, or prognosis, nor should it be used to establish diagnostic or therapeutic cutoffs. Nevertheless, the observed correspondence between greater intralesional thermal heterogeneity and the clinical assessment of greater burn depth in Case 2 warrants further investigation. Therefore, the potential clinical utility of the THP should be prospectively evaluated in larger cohorts using independent clinical outcomes and established reference methods. The research team is currently expanding this investigation through a larger pediatric case series to assess the reproducibility of these findings and determine whether the THP is significantly associated with burn depth, healing time, and clinical outcomes.

6. Study Limitations

This study involves two cases, and the exploratory results cannot be extrapolated. Infrared images were obtained by a trained thermologist, but the image recording angles could not be standardized, which may require a more rigorous protocol. This study has several limitations. First, it is a descriptive case series limited to two pediatric patients; therefore, the findings should be considered exploratory and hypothesis-generating and cannot be generalized to other burn populations. The small sample size precluded inferential statistical analysis, assessment of diagnostic accuracy, or determination of associations between thermal parameters, PLI values, and burn depth or clinical outcomes.

Second, although infrared images were acquired by a trained medical thermologist following the Thermal Burn Protocol, the acquisition angle could not be fully standardized in all anatomical regions because of burn location, patient positioning, and clinical conditions. This may have introduced variability in radiometric measurements. Future studies should incorporate predefined angular tolerances, standardized positioning, and acquisition criteria to improve measurement reproducibility.

Third, the boundaries of the Whole Burn Region of Interest (WB-ROI) were manually delineated by the thermologist in conjunction with the bedside plastic surgeon using the clinically visible burn and the corresponding aligned clinical photograph. Although analysis of the complete WB-ROI avoids the subjective selection of isolated high- and low-temperature regions for quantitative analysis, manual delineation of the burn boundary remains observer-dependent and may introduce segmentation bias. Future studies should therefore assess intraobserver and interobserver reproducibility and investigate semi-automated or automated WB-ROI segmentation. Environmental and physiological factors may also influence skin surface temperature. Wound exposure time, evaporative heat loss, ambient temperature, relative humidity, and airflow represent potential sources of thermal variability. Although a standardized 10-min equilibration period after dressing removal was used before image acquisition, these factors could not be completely controlled under bedside clinical conditions.

Author Contributions

S.M.: conceptualization, methodology, software; S.M.: data curation, writing—original draft preparation; N.G.: visualization, investigation; B.M.: supervision; S.M.: software, validation; G.A., S.M.: writing—reviewing

and editing. L.G. and V.S.: coordination and integration with nursing and medical rounds. All authors have read and agreed to the published version of the manuscript.

Funding:

This research received no external funding.

Institutional Review Board Statement

The ethics committee of the Pereira Rossell Pediatric Hospital approved the conduct of this research on 30 April 2025.

Informed Consent Statement

The clinical cases presented have the endorsement and consent signed by the patients' guardians.

Data Availability Statement

The datasets generated and analyzed during the current study are not publicly available due to patient confidentiality and ethical considerations, particularly given the involvement of pediatric patients. De-identified data may be made available by the corresponding author upon reasonable request, subject to institutional authorization and compliance with applicable ethical and data protection requirements.

Acknowledgments

We would like to thank the Burn and Reconstructive Surgery Unit, Pereira Rossell Pediatric Hospital, Montevideo, Uruguay, for the opportunity to work with a multidisciplinary team.

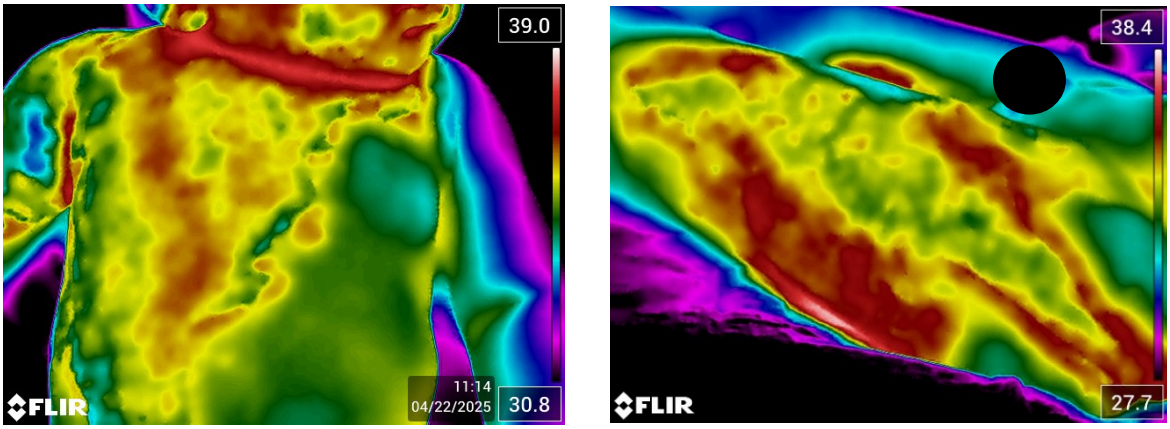
Conflicts of Interest

The authors declare no conflict of interest. Given the role as Editorial Board Member, Sergio Machado had no involvement in the peer review of this paper and had no access to information regarding its peer-review process. Full responsibility for the editorial process of this paper was delegated to another editor of the journal.

Use of AI and AI-Assisted Technologies

No AI tools were utilized for this paper.

Appendix A. Raw Thermal Image IRS and Profile Selection.



References

1. Lee, H.J.; Kim, M. Skin Barrier Function and the Microbiome. *Int. J. Mol. Sci.* **2022**, *23*, 13071. https://doi.org/10.3390/ijms232113071.
2. Zhu, L.; Guo, S.; Wu, P.; et al. Advances in the research of the relationship between wound temperature and wound healing. *Zhonghua Shao Shang Za Zhi* **2018**, *34*, 829–832. https://doi.org/10.3760/cma.j.issn.1009-2587.2018.11.021.
3. Ramirez-GarciaLuna, J.L.; Bartlett, R.; Arriaga-Caballero, J.E.; et al. Infrared thermography in wound care, surgery, and sports medicine: A review. *Front. Physiol.* **2022**, *13*, 838528. https://doi.org/10.3389/fphys.2022.838528.

4. Lanham, J.S.; Nelson, N.K.; Hendren, B.P.; et al. Outpatient Burn Care: Prevention and Treatment. *Am. Fam. Physician* **2020**, *101*, 463–470.
5. Carrière, M.E.; de Haas, L.E.M.; Pijpe, A.; et al. Validity of thermography for measuring burn wound healing potential. *Wound Repair Regen* **2020**, *28*, 347–354. https://doi.org/10.1111/wrr.12786.
6. Burke-Smith, A.; Collier, J.; Jones, I. A comparison of non-invasive imaging modalities: Infrared thermography, spectrophotometric intracutaneous analysis and laser Doppler imaging for the assessment of adult burns. *Burns* **2015**, *41*, 1695–1707. https://doi.org/10.1016/j.burns.2015.06.023.
7. Zhang, H.Y.; Son, S.; Yoo, B.R.; et al. Reference standard for digital infrared thermography of the surface temperature of the lower limbs. *Bioengineering* **2023**, *10*, 283. https://doi.org/10.3390/bioengineering10030283.
8. Son, S.; Yoo, B.R.; Zhang, H.Y. Reference standards for digital infrared thermography measuring surface temperature of the upper limbs. *Bioengineering* **2023**, *10*, 671. https://doi.org/10.3390/bioengineering10060671.
9. Ji S, Xiao S, Xia Z; Consensus on the treatment of second-degree burn wounds (2024 edition). *Burn. Trauma* **2024**, *12*, tkad061. https://doi.org/10.1093/burnst/tkad061.
10. Dang, J.; Lin, M.; Tan, C.; et al. Use of infrared thermography for assessment of burn depth and healing potential: A systematic review. *J. Burn Care Res.* **2021**, *42*, 1120–1127. https://doi.org/10.1093/jbcr/irab108.
11. Martínez-Jiménez, M.A.; Ramirez-GarciaLuna, J.L.; Kolosovas-Machuca, E.S.; et al. Development and validation of an algorithm to predict the treatment modality of burn wounds using thermographic scans: Prospective cohort study. *PLoS ONE* **2018**, *13*, e0206477. https://doi.org/10.1371/journal.pone.0206477.
12. Klama-Baryła, A.; Kitala, D.; Łabuś, W.; et al. Infrared thermal imaging as a method of improving skin graft qualification procedure and skin graft survivability. *Transplant. Proc.* **2020**, *52*, 2223–2230. https://doi.org/10.1016/j.transproceed.2020.01.108.
13. Singer, A.; Relan, P.; Beto, L.; et al. Infrared Thermal Imaging Has the Potential to Reduce Unnecessary Surgery and Delays to Necessary Surgery in Burn Patients. *J. Burn Care Res.* **2015**, *37*, 350–355.
14. Xue, E.Y.; Chandler, L.K.; Viviano, S.L.; et al. Use of FLIR ONE smartphone thermography in burn wound assessment. *Ann. Plast. Surg.* **2018**, *80*, S236–S238. https://doi.org/10.1097/sap.0000000000001363.
15. Ganon, S.; Guédon, A.; Cassier, S.; et al. Contribution of thermal imaging in determining the depth of pediatric acute burns. *Burns* **2020**, *46*, 1091–1099. https://doi.org/10.1016/j.burns.2019.11.019.
16. Simmons, J.D.; Kahn, S.A.; Vickers, A.L.; et al. Early assessment of burn depth with far infrared time-lapse thermography. *J. Am. Coll. Surg.* **2018**, *226*, 687–693. https://doi.org/10.1016/j.jamcollsurg.2017.12.051.
17. Piva, G.; Crepaldi, A.; Zenunaj, G.; et al. The Value of Infrared Thermography to Assess Foot and Limb Perfusion in Relation to Medical, Surgical, Exercise or Pharmacological Interventions in Peripheral Artery Disease: A Systematic Review. *Diagnostics* **2022**, *12*, 3007. https://doi.org/10.3390/diagnostics12123007.
18. Raheman, F.J.; Rojoa, D.M.; Patel, N.G. Performance of infrared thermography and thermal stress test in perforator mapping and flap monitoring: A meta-analysis of diagnostic accuracy. *J. Plast. Reconstr. Aesthetic Surg.* **2021**, *74*, 2013–2025. https://doi.org/10.1016/j.bjps.2021.03.088.
19. Prindeze, N.J.; Fathi, P.; Mino, M.J.; et al. Examination of the Early Diagnostic Applicability of Active Dynamic Thermography for Burn Wound Depth Assessment and Concept Analysis. *J. Burn Care Res.* **2015**, *36*, 626–635. https://doi.org/10.1097/bcr.0000000000000187.
20. Nischwitz, S.P.; Luze, H.; Kamolz, L.P.; et al. Thermal imaging via FLIR One—A promising tool in clinical burn care and research. *Burns* **2020**, *46*, 988–989. https://doi.org/10.1016/j.burns.2020.02.017.
21. Jaspers, M.E.H.; Maltha, I.; Klaessens, J.H.G.M.; et al. Insights into the use of thermography to assess burn wound healing potential: A reliable and valid technique when compared to laser Doppler imaging. *J. Biomed. Opt.* **2016**, *21*, 1. https://doi.org/10.1117/1.jbo.21.9.096006.
22. Asif, A.; Poyiatzis, C.; Raheman, F.J.; et al. The use of infrared thermography (IRT) in burns depth assessment: A diagnostic accuracy meta-analysis. *Eur. Burn. J.* **2022**, *3*, 432–446. https://doi.org/10.3390/ebj3030038.
23. Pedrosa, R.; Souza Martins, L.; Freire, R.M.; et al. Accuracy of infrared thermography evaluation in burn wound healing: A systematic review and meta-analysis. *J. Wound Care* **2024**, *33*, cxviii–cxxix. https://doi.org/10.12968/jowc.2024.33.sup4a.cxviii.
24. Rangaiah, P.K.B.; Pradeep Kumar, B.P.; Huss, F.; et al. Precision diagnosis of burn injuries using imaging and predictive modeling for clinical applications. *Sci. Rep.* **2025**, *15*, 7604. https://doi.org/10.1038/s41598-025-92096-4.
25. Van de Warenburg, M.S.; Wieringa, M.; Ulrich, D.J.O.; et al. The use of the FLIR ONE Pro thermal camera for paediatric burn wound depth assessment: A pilot study. *Burns* **2026**, *52*, 107942. https://doi.org/10.1016/j.burns.2026.107942.
26. Kumar, B.; Patil, N.; Jain, V.; et al. Clinical utility of infrared thermography in pediatric patients: A systematic review of surgical and nonsurgical applications. *J. Indian Assoc. Pediatr. Surg.* **2026**, *31*, 346–362. https://doi.org/10.4103/jiaps.jiaps_413_25.

27. de Haan, J.; Stoop, M.; van Zuijlen, P.P.M.; et al. Thermal imaging for burn wound depth assessment: A mixed-methods implementation study. *J. Clin. Med.* **2024**, *13*, 2061. https://doi.org/10.3390/jcm13072061.
28. Hardwicke, J.; Thomson, R.; Bamford, A.; et al. A pilot evaluation study of high resolution digital thermal imaging in the assessment of burn depth. *Burns* **2013**, *39*, 76–81. https://doi.org/10.1016/j.burns.2012.03.014.